Available online at www.sciencedirect.com
SCIENCE DIRECT
Lithos 87 (2006) 80–103
LITHOS
www.elsevier.com/locate/lithos

Geochemistry of volcanic rocks from the Geysers geothermal area, California Coast Ranges

Axel K. Schmitt [a,*], Rolf L. Romer [b], James A. Stimac [c]

[a] *Department of Earth and Space Sciences, University of California, Los Angeles, 595 Charles Young Drive E, Los Angeles Ca 90095-1567, U.S.A.*
[b] *Geoforschungszentrum Potsdam, Germany*
[c] *Philippine Geothermal, Inc., Makati, Philippines*

Received 1 May 2004; accepted 25 May 2005
Available online 1 August 2005

Abstract

The Geysers geothermal reservoir in the California Coast Ranges is the world's largest economically used geothermal system. Surface exposure of volcanic rocks and extensive drill penetration of a >300 km^3 subsurface plutonic body (Geysers Plutonic Complex or GPC) that underlies the reservoir allow unique insights into the evolution of a volcanic–plutonic magma system. We present compositional data for major elements, trace elements, and Nd, Sr and Pb isotopes of late Pliocene to early Pleistocene lavas that are spatially related to the geothermal reservoir and cores from coeval subsurface plutonic rocks. Isotopic ratios of dacitic to rhyolitic lavas from Cobb Mountain, Pine Mountain and Tyler Valley, and core samples from the shallow microgranite phase of the GPC range between 0.70343–0.70596 ($^{87}Sr/^{86}Sr$), 0.512813–0.512626 ($^{143}Nd/^{144}Nd$), and 19.084–19.189 ($^{206}Pb/^{204}Pb$). These compositions fall between values for two major isotopic end-members: (1) coeval basalt of Caldwell Pines that has compositional affinities to magmas extracted from a subcontinental mantle-wedge, and (2) regional crustal rocks equivalent to those of the Franciscan and Great Valley sequence. Model calculations suggest that lower crustal intrusion of basalt triggered crustal assimilation in mass proportions of ~5 : 1 to produce magmas of intermediate composition. Because rhyolites are isotopically indistinguishable to dacites, we interpret them as partial melts derived from precursor intrusions of granodioritic compositions. Our data suggest that two major mantle and crustal reservoirs continually interacted over the >1 Ma duration of volcanism and pluton emplacement at the Geysers. Individual magma pulses, however, evolved independently, arguing against the presence of a single long-lived magma body.

Keywords: The Geysers; California Coast Ranges; Clear Lake volcanics; Magmatic evolution; Crustal contamination; Geochemistry; Sr–Nd–Pb isotopes

1. Introduction

Geothermal activity at the Geysers, the world's largest single source of geothermal energy, is ulti-

* Corresponding author. Tel.: +1 310 206 5760.
E-mail address: axel@argon.ess.ucla.edu (A.K. Schmitt).

0024-4937/$ - see front matter © 2005 Published by Elsevier B.V.
doi:10.1016/j.lithos.2005.05.005

mately driven by localized high near-surface heat-flow within a 100 × 50 km thermal anomaly located in the Northern California Coast Ranges (Walters and Combs, 1992). Over the past two decades, evidence from geothermal well drilling emerged that the Geysers geothermal reservoir is localized above and within a concealed plutonic body, the Geysers Plutonic Complex or GPC (e.g., Schriener and Suemnicht, 1980; Hulen and Nielson, 1993, 1996). The extent of the GPC spatially correlates with surface outcrops of Cobb Mountain and smaller volcanic centers to the NW and SE of Cobb Mountain (Fig. 1). Radiometric ages for these centers range from ~2.1 to 0.7 Ma (Donnelly-Nolan et al., 1981; Schmitt et al., 2003a) and recent U–Pb dating of zircon from geothermal wells (Dalrymple et al., 1999; Schmitt et al., 2003b) further reveals that the GPC assembled in a piecemeal fashion between ~1.8 and 1.1 Ma. These geochronologic data suggest that younger magmatic heat sources for the present-day steam field might be concealed in the subsurface (cf., Schriener and Suemnicht, 1980).

While the nature of the present-day heat source remains uncertain, our study of the GPC and related volcanic rocks aims at a better understanding of the role of mantle-derived magmas and the nature of episodic magmatic pulses that collectively resulted in a long-lived thermal anomaly (Moore and Gunderson, 1995; Dalrymple et al., 1999; Norton and Hulen, 2001; Stimac et al., 2001). We concentrate on volcanic rocks overlying the GPC for which previous high-spatial resolution dating studies confirmed a close genetic relation to the main-phase GPC intrusives (Schmitt et al., 2003a,b). This is because drilling of the GPC was mostly conducted with air instead of water, and therefore GPC cuttings are generally too fine-grained (<1 mm) to allow uncontaminated sampling. The exceptions are two samples from one of the rare core samples drilled into the central portion of the

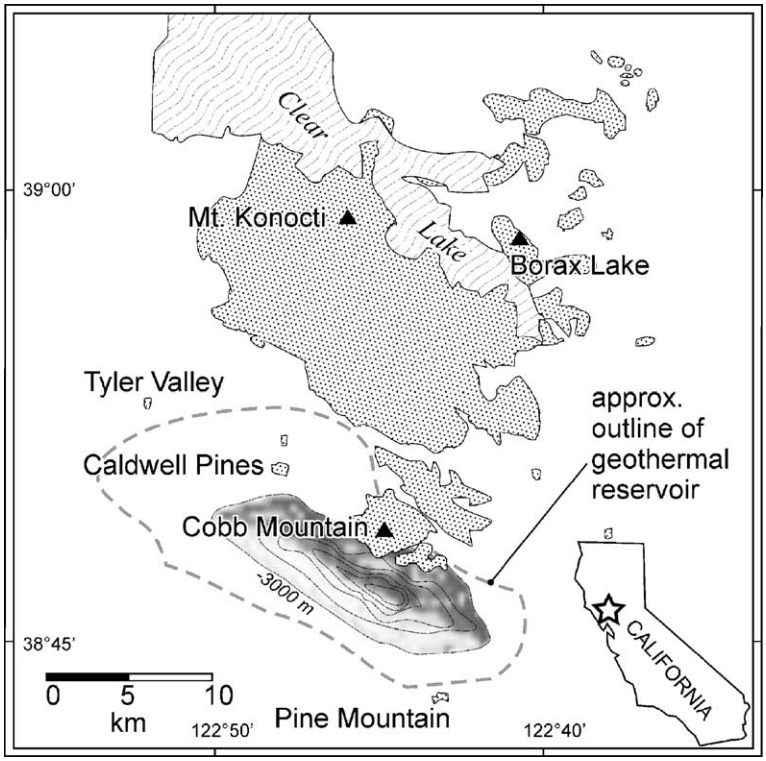

Fig. 1. Geologic sketch map showing surface distribution of Clear Lake volcanic rocks (stippled fields; modified from Hearn et al., 1981) and subsurface extent of the Geysers Plutonic Complex (GPC; shaded relief with depth isolines in meters below sea-level extending from −3000 to −500 m.b.sl.; Norton and Hulen, 2001). Surface-projected extent of the Geysers geothermal reservoir and localities mentioned in text are indicated.

GPC (well GDC21) and we included them for chemical analysis.

New trace element and radiogenic isotope (Sr, Nd, Pb) data allow us to reassess the amounts of mantle-derived material in the Geysers magmas. Model calculations using algorithms by Aitcheson and Forrest (1994), Spera and Bohrson (2001), and Bohrson and Spera (2001) indicate that large-volume intrusions of mantle-derived basalt are concealed in the lower crust beneath the Geysers despite the fact that eruption of basalt was volumetrically subordinate (Donnelly-Nolan et al., 1981). Assimilation– fractional crystallization at lower crustal levels (>1000 MPa) generated hybrid intermediate magmas, whereas rhyolites may have formed by remelting of consanguineous granodioritic intrusions at shallow-levels. This general model for two stages of magma evolution at deep and shallow-levels is similar to that proposed by Stimac et al. (2001) based on broad petrographic and chemical studies of younger silicic volcanic centers within the Clear Lake area, and agrees with geophysical models for the generation of voluminous basaltic magmas in the trail of the migrating Mendocino triple junction (Liu and Furlong, 1992; Liu, 1993; Guzofski and Furlong, 2002).

2. Geological background

2.1. Volcanism in the California Coast Ranges

A series of volcanic fields that were active primarily along the eastern side of the San Andreas Fault throughout the Late Cenozoic occurs within the California Coast Ranges (Hearn et al., 1981). Moving northwestward from the oldest volcanic remnants preserved in the San Francisco Bay area (Dickinson, 1997), the focus of magmatism within the California Coast Ranges has shifted to its present location around Clear Lake over the last ~15 Ma. The onset of volcanism spatially correlates with the relative movements of the Mendocino triple junction that separates the Pacific–North American transform in the south from subduction of the Juan de Fuca plate beneath North America in the north (Dickinson and Snyder, 1979; Johnson and O'Neil, 1984; Fox et al., 1985; Dickinson, 1997).

Modeling of mantle-flow indicates that a transient pulse of elevated heat-flow and volcanism in the Coast Ranges is caused by asthenospheric upwelling in the slab-free window as subduction ceases in the wake of the NW-migrating Mendocino triple junction (Liu and Furlong, 1992; Liu, 1993; Goes et al., 1997; Stimac et al., 2001; Guzofski and Furlong, 2002). It remains a matter of debate if Coast Range basaltic magmas are derived from depleted suboceanic mantle with some amount of crustal contamination (e.g., Cole and Basu, 1995) or if they originated from subcontinental mantle (e.g., Johnson and O'Neil, 1984). In general, however, the amount of basaltic lavas is low and individual fields are dominated by calc-alkaline dacites to rhyolites (Donnelly-Nolan et al., 1981, 1993).

2.2. Clear Lake volcanic field

The Geysers geothermal reservoir sits astride the southwestern margin of the Clear Lake Volcanic field, the youngest among the Coast Range volcanic fields. Volcanism started S of the Geysers area during the late Pliocene and the most recent activity occurred along the shores of Clear Lake, about ~20 km N of the Geysers geothermal reservoir, until about 0.01–0.1 Ma ago (Hearn et al., 1981; Sarna-Wojcicki et al., 1981). The Clear Lake Volcanic field is thought to have formed by crustal extension related to pull-apart basin formation within the San Andreas transform fault system over a slab-free window (Donnelly-Nolan et al., 1993).

There is general consensus that more evolved magmas in the Clear Lake area and other Coast Range volcanic fields are affected by significant degrees of crustal contamination (e.g., Dickinson, 1997). For example, oxygen, strontium and neodymium isotopic data clearly indicate a significant crustal component in Coast Range dacites and rhyolites (Futa et al., 1981; Johnson and O'Neil, 1984; Hammersley and DePaolo, 1999). Moreover, crustal xenolithic inclusions are common in Clear Lake basalts and andesites (e.g., Hearn et al., 1981). These xenoliths are dominated by orthopyroxene and plagioclase with lesser garnet, biotite, ilmenite, cordierite, and sillimanite. They likely represent high-grade metamorphic equivalents of Franciscan or Great Valley Sequence sedimentary rocks, with some having residual compositions after

extraction of partial melt (Stimac, 1993). Chilled magmatic inclusions consisting of mafic mineral aggregates are a second type of inclusion that is ubiquitous in many Clear Lake silicic volcanic rocks (Stimac, 1991; Stimac and Pearce, 1992). Their presence suggests that mixing between basaltic and more evolved magmas occurred prior to eruption. Late-stage recharge with more primitive magma is further supported by $^{87}Sr/^{86}Sr$ heterogeneities between feldspar phenocrysts and whole-rock analyses (Futa et al., 1981).

2.3. The Geysers plutonic complex and related volcanic units

The Geysers is unique among Coast Range volcanic centers because samples of subvolcanic intrusives are available from geothermal well drilling. Schriener and Suemnicht (1980) first described that a hypabyssal plutonic body underlies the Geysers steam reservoir. While early literature frequently refers to this body as the 'Felsite', we prefer the term Geysers Plutonic Complex (GPC) in recognition of its composite nature. The northwest trending antiformal shape of the GPC coincides with an early high-temperature hydrothermal aureole (Thompson, 1992; Moore and Gunderson, 1995) and the present-day steam reservoir, both located in country rocks mainly composed of metamorphic greywacke of the Mesozoic Franciscan subduction complex (Fig. 1; McLaughlin and Donnelly-Nolan, 1981; Hearn et al., 1995). Geothermal wells that reach up to ~3 km depth have not penetrated through the GPC.

Within the GPC, three major compositional and structural units can be distinguished: (1) microgranite porphyry, (2) orthopyroxene–biotite granite, and (3) hornblende–biotite granodiorite (Hulen and Nielson, 1993, 1996). Microgranite porphyry forms the shallow cupola of the GPC that is first encountered at a depth of ~700 m below the surface (or approximately at sea-level; Fig. 1). Orthopyroxene–biotite granite and hornblende–biotite granodiorite comprise the deeper portions of the GPC that broadens downward to a width of 3 km at ~3000 m below sea-level. Drilling also encountered granitic dikes within the country rocks that overlie the main body of the GPC whose thickness typically range between a few centimeters to a few meters.

Volcanic rocks that directly overly the GPC occur within isolated centers, the largest of which is Cobb Mountain (Fig. 1). Compared to the GPC, the volcanic rocks display a wider compositional range. The Cobb Mountain sequence, for example, comprises early andesite (Ford Flat), overlain by rhyolite (Alder Creek), rhyodacite (Cobb Mountain), and dacite (Cobb Valley; type localities in parentheses). The most primitive magma erupted in the area is basalt of Caldwell Pines which crops out in the NW portion of the geothermal field. In our study, we also include two small volcanic centers that are located adjacent to the surface-projected extent of the GPC: Pine Mountain and Tyler Valley (Fig. 1). Two distinct units, rhyolite of Pine Mountain and rhyodacite of Turner Flat were distinguished at Pine Mountain, whereas Tyler Valley is mapped as a single dacite flow or plug (Hearn et al., 1995).

Together with Cobb Mountain, these three centers are broadly arranged parallel to the NW–SE trending extension of the underlying GPC. They also show progressively younger eruption ages from SE to NW, based on the $^{40}Ar/^{39}Ar$ results of Schmitt et al. (2003a): 2.17 ± 0.02 Ma (rhyolite of Pine Mountain), 1.16 ± 0.02 to 1.00 ± 0.05 Ma (Cobb Mountain sequence) and 0.67 ± 0.01 (Tyler Valley). Additional insight into the timing of intrusive and extrusive events at the Geysers comes from U–Pb zircon dating (Schmitt et al., 2003a,b). Zircons from rhyolite of Pine Mountain and dacite of Tyler Valley yielded average U–Pb ages (2.46 ± 0.03 Ma and 0.95 ± 0.03 Ma, respectively) that have no age overlap with Cobb Mountain or GPC zircons. They therefore likely evolved as separate magmatic centers. The oldest unit within the GPC comprises shallow orthopyroxene–biotite granite (1.67 ± 0.05–1.91 ± 0.04 Ma; Schmitt et al., 2003b), which has no age equivalent in the zircon population of any of the studied volcanic units. In contrast, the deeper portions of the GPC (orthopyroxene–biotite granite and hornblende–biotite granodiorite) have average U–Pb zircon ages (1.11 ± 0.03–1.46 ± 0.03 Ma; Schmitt et al., 2003b) that overlap with those for Cobb Mountain units (1.26 ± 0.02–1.35 ± 0.01 Ma; Schmitt et al., 2003a), supporting the notion from compositional data that they are eruptive equivalents of intrusive rocks of the GPC (e.g., Hulen and

Nielson, 1996). The age of basalt of Caldwell Pines is constrained by a whole-rock K–Ar result (1.66 ± 0.12 Ma; Donnelly-Nolan et al., 1981). Despite the relatively large uncertainty, this result suggests that basaltic volcanism falls close to the upper ranges of GPC ages.

The unique subsurface exploration of plutonic rocks coupled with preservation of volcanic materials at the Geysers allows constraining the intrusive and extrusive volumes of the magma system. Cobb Mountain, the largest of these early Clear Lake centers, comprises only ~5 km^3 of mostly rhyolitic lava (Hearn et al., 1995). Caldwell Pines, Pine Mountain, and Tyler Valley are even smaller in volume (<0.1 km^3; Hearn et al., 1995). The estimated volume of the GPC (~300 km^3; Norton and Hulen, 2001) in contrast dwarfs that of volcanic rocks overlying the Geysers reservoir and translates into extrusive/intrusive ratio for the Geysers magma system of <1:60. This ratio is unusually low in as much it is smaller than both the 1:10 ''rule of thumb'' value of Smith and Shaw (1975, 1978) and the <1:16 estimates by Spera and Crisp (1981) and Crisp and Spera (1984) that are based on theoretical considerations. In this context it is noteworthy that Stimac et al. (2001) estimate similarly small extrusive/intrusive volume ratios of 1:35 to <1:50 from thermal modeling of younger Clear Lake centers at Mt. Konocti and Borax Lake (see Fig. 1).

3. Sample selection and methods

We geochemically analyzed whole-rocks from major eruptive units of Cobb Mountain, Pine Mountain, Caldwell Pines and Tyler Valley, and include analyses of quartz-hosted melt inclusions from rhyolite of Alder Creek. Rhyolite of Alder Creek is one of the most voluminous silicic units in the area, and the melt inclusion record provides insights into the genesis of evolved rhyolitic magmas that constitute a significant portion of the GPC. Country rock samples comprising non-reservoir greywacke and serpentinite were included as potential source or assimilant rocks. In addition, we selected a core sample from the GPC (GDC21-5865) that was also used in a previous zircon dating study (Schmitt et al., 2003b). Based on these results, GDC21-5865 is equivalent to the early ~1.8 Ma microgranite porphyry phase of the GPC. GDC21-5865 shows centimeter-scale textural heterogeneity in which a coarse grained dike intruded a fine-grained matrix. By dissecting the core with a diamond wafer saw and separately crushing the individual parts, we obtained samples for chemical analyses of the dike

Table 1a
Selected electron microprobe analyses of feldspar rims for Geysers volcanic rocks

Sample	PM-01-02 rhyolite of Pine Mtn.		CM-00-02 rhyolite of Alder Creek		CM-00-03 rhyodacite of Cobb Valley		CM-00-04 rhyodacite of Cobb Mtn.		TV-01-01 dacite of Tyler Valley	
Phase	pl	san	pl	san	pl	San	pl	san	Pl	san
wt.%										
SiO_2	64.0	66.1	62.9	65.5	52.7	65.4	63.2	66.3	61.8	65.7
Al_2O_3	22.7	19.0	23.0	18.7	29.9	18.9	22.7	19.0	24.3	18.9
FeO total	0.12	0.04	0.11	0.06	0.06	0.03	0.11	0.07	0.08	0.03
CaO	4.21	0.14	4.67	0.20	12.69	0.47	4.61	0.21	6.21	0.19
Na_2O	8.63	3.81	8.39	3.67	4.24	5.44	8.47	4.41	7.45	3.72
K_2O	1.10	10.9	1.08	11.1	0.17	8.28	1.18	10.1	0.95	10.8
BaO	0.06	0.93	0.06	0.57	0.01	0.96	0.03	0.65	0.02	1.19
Total	100.8	100.9	100.3	99.7	99.8	99.5	100.3	100.7	100.7	100.6
$T_{san\text{-}pl}$ [°C]										
Ab	763		771		–		822		821	
Or	751		774		–		794		800	
An	749		780		–		822		824	

$T_{san\text{-}pl}$ = Two-feldspar thermometry results for average feldspar rim compositions using the Ab, Or, and An calibration of the Green and Usdansky (1986) thermometer at 200 MPa with an approximate uncertainty of ± 40 °C. No temperatures were calculated for CM-00-03 because of strong heterogeneity of feldspar rim compositions.

Table 1b
Selected electron microprobe analyses of orthopyroxene for Geysers volcanic rocks

Sample	CM-00-02 rhyolite of Alder Creek		CM-00-03 rhyodacite of Cobb Valley	
Phase	opx	opx	opx	opx
wt.%				
SiO_2	51.8	49.6	56.3	49.7
TiO_2	0.17	0.07	0.14	0.10
Al_2O_3	1.01	0.24	1.45	0.19
Cr_2O_3	0.11	0.01	0.31	0.00
FeO total	26.5	35.6	11.0	35.3
MnO	0.44	1.26	0.23	1.39
MgO	19.3	12.7	30.6	12.6
CaO	0.95	0.7	0.75	0.94
Na_2O	0.05	0.01	0.03	0.03
Total	100.4	100.2	100.8	100.3
Mol%				
Wo	1.9	1.5	1.4	2.0
En	54.9	37.6	81.8	37.1
Fs	43.1	60.9	16.8	60.9

and the matrix (GDC21-5865-D and GDC21-5865-M, respectively).

Mineral and melt inclusion compositions (including trace elements) were analyzed in hand-picked crystal separates by microanalytical methods using the Cameca SX100 electron microprobe (EPMA) and micro-infrared spectroscopy (FTIR) at the GeoForschungsZentrum Potsdam (GFZ) and the Cameca ims1270 high-resolution ion microprobe (SIMS) at the University of California, Los Angeles (UCLA; see Schmitt et al., 2001 for analytical procedures).

With the exception of the core sample GDC21 (total mass ~250 g), whole-rock samples comprised several kilograms of rock. Weathered rinds were chipped off by a hammer and cleaned samples were crushed in a jaw crusher. Aliquots of the crushed rock chips were then finely ground in an agate mill, or further sieved for mineral separation by hand-picking. Powdered samples were used for quantitative X-ray diffraction (XRD) analysis to determine rock modal compositions (Emmermann and Lauterjung, 1990). Analytical details for quantitative X-ray fluorescence (XRF) and mass spectrometry with inductively coupled plasma (ICP-MS) can be found in Trumbull et al. (1999) and for optical spectrometry with inductively coupled plasma ICP-OES in Kasemann et al. (2001). All isotopic ratios were determined at the GFZ. Lead isotopic ratios were measured at 1200–1250 °C on a Finnigan MAT262 multicollector mass-spectrometer using static multicollection. Instrumental fractionation was corrected with 0.1% per a.m.u. as determined from repeated measurement of lead reference-material NBS 981. Accuracy and precision of reported Pb ratios are better than 0.1% at the 2-σ level. Total procedural blanks for whole-rock samples are better than 30 pg Pb. Sr was loaded on single Ta-filaments and its isotopic composition was determined on a VG 54-30 Sector multicollector mass-spectrometer using a triple-jump dynamic multicollection setup. $^{87}Sr/^{86}Sr$ data are normalized with $^{86}Sr/^{88}Sr=0.1194$. Repeated measurement of Sr standard NBS 987 during the measurement period gave 0.710253 ± 0.000010 (2σ, $n=6$). Analytical uncertainties of the individual measurements are reported as $2\sigma_m$. Total procedural blanks are less than 50 pg Sr. Nd was loaded on double Re-filaments and its isotopic composition was measured on a Finnigan MAT262 multicollector

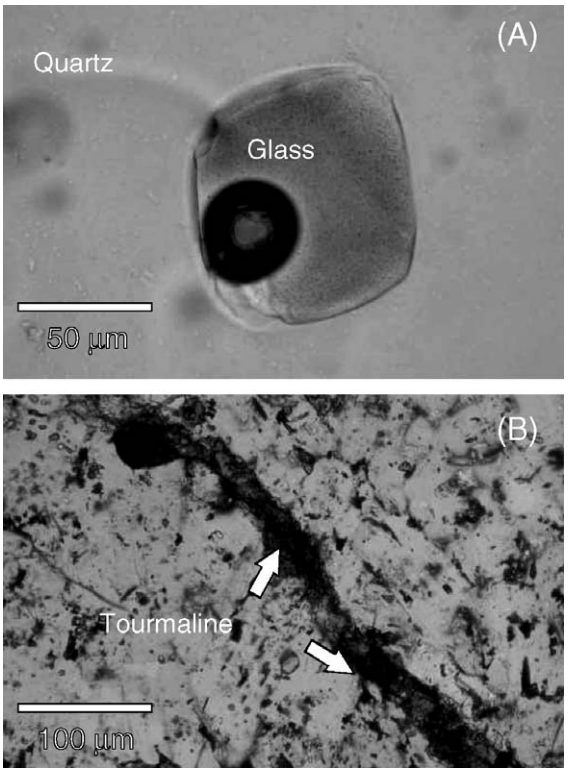

Fig. 2. (A) Moderately devitrified melt inclusion in quartz (rhyolite of Alder Creek; CM0002). (B) Tourmaline vein in microgranite porphyry (GDC21-5865-D).

mass-spectrometer using dynamic multicollection. $^{143}Nd/^{144}Nd$ data are normalized with $^{146}Nd/^{144}Nd = 0.7219$. Repeated measurement of La Jolla Nd standard during the measurement period gave $^{143}Nd/^{144}Nd = 0.511853 \pm 0.000005$ (2σ, $n = 8$). Analytical uncertainties of the individual measurements are reported as $2\sigma_m$. Total procedural blanks are less than 30 pg Nd.

4. Petrography

4.1. Volcanic rocks

All silicic volcanic samples here studied have similar phenocryst assemblages dominated by sodic plagioclase, sanidine, and quartz with lesser orthopyroxene, biotite, and occasionally clinopyroxene. XRD

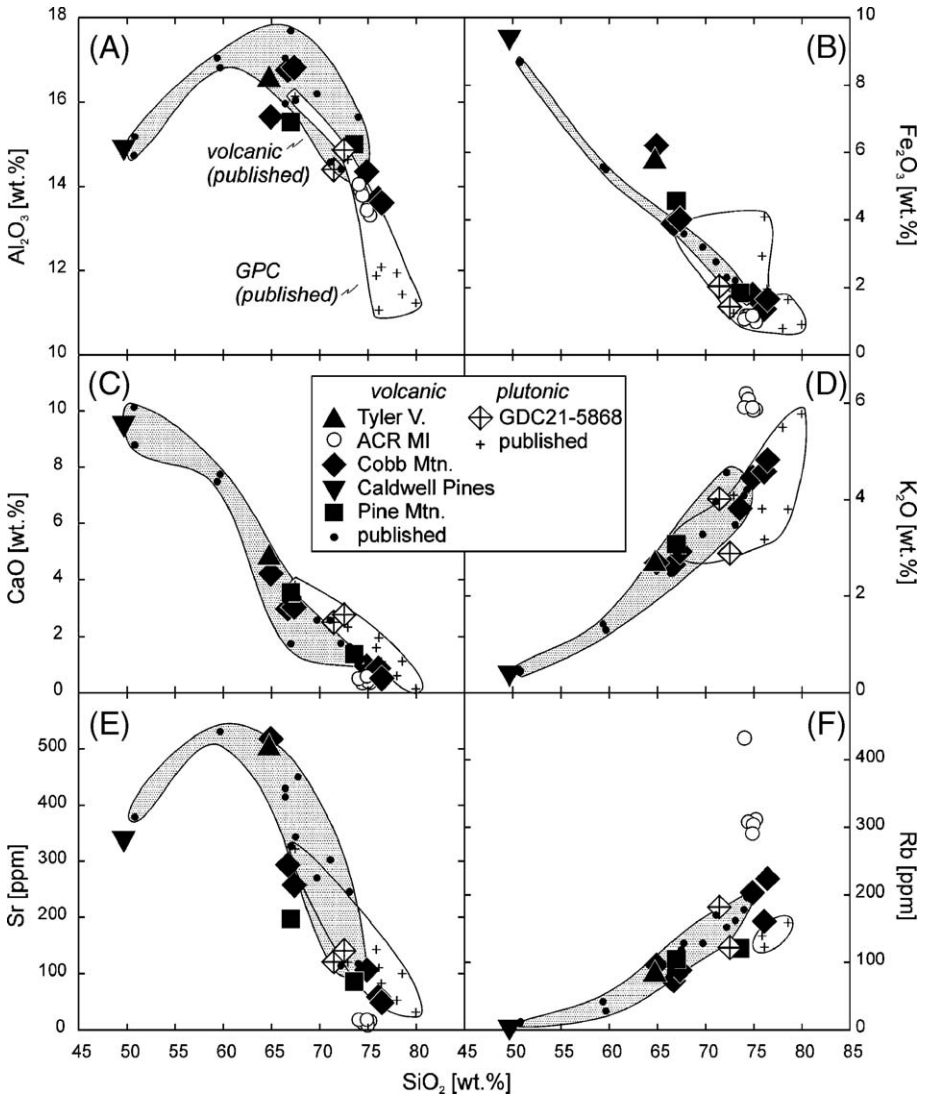

Fig. 3. SiO_2 variation diagrams for selected major elements and trace elements showing whole-rock and melt inclusion analyses. Abbreviations used: Tyler V. = dacite of Tyler Valley; ACR MI = rhyolite of Alder Creek melt inclusions; Cobb Mtn. = Cobb Mountain units (in stratigraphic order: rhyolite of Alder Creek, rhyodacite of Cobb Mountain, dacite of Cobb Valley); Pine Mtn. = rhyolite and dacite of Pine Mountain; Caldwell Pines = basalt of Caldwell Pines). Fields indicate range of published results for Geysers volcanic (stippled; Hearn et al., 1981; Stimac, 1991; Goff et al., 2001) and plutonic rocks (open; Hulen and Nielson, 1993; Schmitt et al., 2003a). Published data are shown as small symbols.

analysis and visual inspection indicate subequal amounts of quartz, plagioclase (typically An_{18}–An_{29}; Table 1a), and sanidine (Or_{64}–Or_{69}; Table 1a) in the rhyolites. Plagioclase (50–56% by XRF; compositional range between An_{21} and An_{62}; Table 1a) is the dominant crystal phase in the dacites and rhyodacites. Orthopyroxene (between En_{38} and En_{55}; Table 1b) makes up <5% of the crystal phases. Main accessory phases present in heavy mineral separates are apatite, zircon, and sphene. In addition to the above minerals, all volcanic units contain sparse phenocrysts of ilmenite, commonly in aggregates with the ferromagnesian minerals. Strong devitrification of the matrix is ubiquitous in all silicic units. Some only moderately devitrified melt inclusions, however, are preserved in quartz phenocrysts from rhyolite of Alder Creek (Fig. 2).

The most primitive sample analyzed is basalt of Caldwell Pines. Chromite-bearing olivine ($Fo_{88–90}$) and clinopyroxene ($Wo_{45}En_{50}Fs_5$) were identified as the dominant phenocryst phases. Calcic plagioclase phenocrysts (An_{80}) are rare. Plagioclase, however, is common as a microphenocrystic phase and comprises ~78% of the rock, compared to 16% clinopyroxene and 6% olivine, as determined by XRD analysis.

Our field observations indicate that basalt of Caldwell Pines is one of the few mafic rocks at Clear Lake that lacks observable xenocrysts of crustal rocks. Elsewhere in the Clear Lake area, however, xenoliths are abundant in basalts and basaltic andesites and comprise high-grade metamorphic rocks with complexly overprinted fabrics and partial melting textures, as well as noritic to gabbroic rocks with cumulate textures (Stimac, 1993). Metapelitic xenoliths record progressive recrystallization and partial melting reactions which have increased the modal proportions of cordierite, plagioclase, orthopyroxene, and ilmenite at the expense of garnet, sillimanite, and biotite. The lack of K-feldspar and quartz in many pelitic xenoliths was attributed to removal of these phased through partial melting (Stimac, 1993). Temperature and pressure estimates for metamorphic xenoliths range from ~750–900 °C and 440–760 MPa, or depths of 12 to 18 km (Stimac, 1993). In this context, it should be mentioned that the dominance of ilmenite over magnetite in Clear Lake dacites and rhyolites presumably reflects the bulk composition and low fO_2 of the metasedimentary source regions (Stimac and Hickmott, 1994).

Many of the Clear Lake silicic lavas also contain small quenched andesitic inclusions (<2 cm) and their disaggregation products (Stimac and Pearce, 1992). Typically, the percentage of andesitic inclusions is lower in the rhyolites compared to the dacites. Their mineral compositions differ from those of phenocrystic orthopyroxene given in Table 1b (plag<An_{81}; clinopyroxene $Wo_{41}En_{51}Fs_8$; magnesian orthopyroxene $Wo_2En_{86}Fs_{12}$; Stimac and Pearce, 1992).

4.2. Plutonic rocks

Plutonic rocks from the GPC share petrographical and mineralogical characteristics of associated silicic volcanic rocks such as the abundance of porphyritic feldspar and quartz. Orthopyroxene and biotite are abundant, but relative proportions vary (Hulen and Nielson, 1993, 1996). As with the volcanic rocks, the GPC rocks contain ilmenite as the dominant FeTi oxide mineral.

Only plutonic rocks, however, feature late-stage minerals and secondary hydrothermal phases (tourmaline, albite, epidote, chlorite), especially in intensely altered shallow microgranite porphyry. Even in relatively fresh samples, such as in core GDC21-5865, abundant secondary tourmaline is present that either appears to replace biotite or that occurs in cross-cutting veins (Fig. 2B). Individual calcic zones ($An_{64–80}$) in generally more sodic plagioclase have been described in orthopyroxene–biotite granite and hornblende–biotite granodiorite samples and suggest involvement of mafic magma in the petrogenesis of plutonic rocks (Norton and Hulen, 2001).

5. Results

5.1. Whole-rock major and trace element compositions

In Fig. 3 and Tables 2 and 3, we summarize new and published whole-rock and melt inclusion compositional data for the Geysers intrusive complex and Clear Lake volcanic rocks that were selected

Table 2
Whole-rock major and trace element compositions and isotopic ratios of Sr, Nd and Pb

Sample	CM-00-01[a]	CM-00-02[b]	ACR2	CM-00-03[b]	CM-00-04[b]	CM-01-01[a]	PM-01-01[a]	PM-01-02[b]	CP-01-01	TV-01-01[b]	CM-02-01	CM-02-02	GDC21-5865-M[b]	GDC21-5865-D[b]
Type	Rhyolite	Rhyolite	Rhyolite	Rhyodacite	Rhyodacite	Rhyodacite	Rhyodacite	Rhyolite	Basalt	Dacite	Serpentinite	Graywacke	GPC	GPC
Unit	Alder Creek	Alder Creek	Alder Creek	Cobb Valley	Cobb Mtn.	Cobb Mtn.	Turner Flat	Pine Mtn.	Caldwell Pn.	Tyler Valley	Franciscan	Franciscan	Microgranite	Microgranite
Longitude W	122°45′ 584	122°46′ 000	122°45′ 117	122°43′ 280	122°42′ 750	122°43′ 167	122°41′ 517	122°41′ 700	122°48′ 933	122°54′ 083	122°46′ 425	122°46′ 027	122°45′ 010	122°45′ 010
Latitude N	38°48′ 766	38°48′ 820	38°48′ 767	38°49′ 420	38°48′ 950	38°47′ 983	38°44′ 005	38°44′ 005	38°50′ 500	38°52′ 283	38°48′ 775	38°48′ 378	38°46′ 460	38°46′ 460
wt.%														
SiO_2	73.5	74.7	75.3	65.5	66.0	64.4	65.5	72.4	49.3	63.2	39.2	68.4	70.5	71.5
TiO_2	0.23	0.18	0.23	0.56	0.66	0.53	0.42	0.34	0.62	0.50	0.02	0.61	0.25	0.25
Al_2O_3	14.1	13.5	13.4	16.5	16.5	15.	15.2	14.8	14.8	16.1	0.62	12.8	14.2	14.6
Fe_2O_3 total	1.76	1.34	1.63	3.83	3.95	6.16	4.47	1.81	9.37	5.59	9.17	4.99	2.02	1.41
MnO	0.03	0.03	0.01	0.05	0.07	0.08	0.06	0.01	0.15	0.08	0.08	0.07	0.03	0.02
MgO	0.44	0.22	0.20	2.51	1.64	2.29	2.22	0.56	12.9	1.50	37.5	2.84	1.10	0.65
CaO	0.91	0.83	0.48	2.91	2.98	4.19	3.48	1.35	9.50	4.66	0.07	1.86	2.46	2.72
Na_2O	2.82	2.92	2.47	3.66	3.26	3.19	3.27	3.38	2.14	3.20	0.03	2.86	4.05	4.42
K_2O	4.37	4.49	4.75	2.60	2.86	2.66	3.01	3.75	0.41	2.59	<0.01	1.91	3.96	2.84
P_2O_5	0.04	0.03	0.04	0.14	0.14	0.15	0.16	0.09	0.10	0.12	0.02	0.13	0.15	0.13
H_2O	1.35	1.02	1.63	1.36	1.68	0.71	1.43	0.95	0.40	1.19	12.74	2.95	0.48	0.46
CO_2	0.09	0.06	0.11	0.10	0.13	0.20	0.77	0.09	0.14	1.56	0.14	0.58	0.49	0.49
Total	99.6	99.3	100.2	99.7	99.8	100.1	99.9	99.5	99.9	100.3	99.6	100.1	99.8	99.5
ppm														
Li	–	50	81	29	22	–	–	36	9	22	0.3	18	–	–
B	–	83	58	26	28	–	–	42	5	37	40	32	662	502
Sc	–	3.4	4.1	10	11	–	–	5.8	26	12	5.5	13	–	–
V	13	b.d.	13	57	57	84	48	21	161	83	41	115	20	13
Cr	b.d.	b.d.	b.d.	92	b.d.	89	110	37	651	68	3080	159	33	29
Ni	b.d.	b.d.	10	45	b.d.	31	47	20	300	31	2728	72	20	14
Zn	28	24	23	56	50	43	45	18	53	41	40	70	24	15
Rb	203	161	224	73	88	96	105	121	5.0	82	0.1	60	182	122

Sr	106	58	49	293	257	518	198	85	341	500	1.6	73	120	141
Y	–	19	16	57	18	–	–	15	12	18	b.d.	15	34	24
Nb	7.0	5.8	7.9	5.8	6.9	–	–	6.1	2.4	5.8	0.11	8.1	–	–
Zr	118	114	136	150	146	118	136	139	58	124	12	132	109	97
Ba	774	768	593	837	807	644	677	834	134	871	10	399	431	281
Pb	22	23	26	19	16	–	–	22	2.3	13	0.04	9.3	19	14
La	–	26	24	49	21	–	–	19	5.4	19	b.d.	20	32	13
Ce	–	42	40	39	40	–	–	34	12	37	b.d.	35	64	29
Pr	–	4.7	5.0	10	4.9	–	–	4.3	1.7	5.0	b.d.	4.9	7.1	3.7
Nd	–	15	16	42	19	–	–	15	7.4	17	b.d.	17	25	14
Sm	–	3.0	3.1	8.4	4.0	–	–	3.3	1.9	3.5	b.d.	3.3	5.5	3.5
Eu	–	0.38	0.30	2.8	1.0	–	–	0.62	0.71	0.79	b.d.	0.82	0.40	0.34
Gd	–	2.8	2.8	8.1	3.6	–	–	3.0	2.0	3.2	b.d.	2.9	5.4	3.5
Tb	–	0.54	0.51	1.3	0.63	–	–	0.55	0.39	0.57	b.d.	0.51	0.93	0.62
Dy	–	2.9	2.6	6.8	3.3	–	–	2.8	2.1	2.9	b.d.	2.6	5.9	4.0
Ho	–	0.57	0.49	1.5	0.63	–	–	0.51	0.40	0.57	b.d.	0.51	1.2	0.83
Er	–	1.8	1.6	4.4	1.9	–	–	1.6	1.3	1.7	b.d.	1.6	3.5	2.5
Tm	–	0.28	0.26	0.65	0.27	–	–	0.23	0.18	0.25	b.d.	0.23	0.51	0.37
Yb	–	1.9	1.7	4.0	1.9	–	–	1.6	1.2	1.7	b.d.	1.6	3.3	2.5
Lu	–	0.29	0.26	0.64	0.29	–	–	0.24	0.19	0.26	b.d.	0.25	0.46	0.37
Th	20	21	24	8.6	12	–	–	11.6	1.3	11	b.d.	6.1	13	16
U	7.7	7.4	6.9	3.5	4.3	–	–	3.7	0.5	3.7	b.d.	1.9	5.9	7.9
$^{87}Sr/^{86}Sr_i$	–	0.70437±1	0.70425±1	0.70515±1	0.70424±1	–	–	0.70517±1	0.70297±1	0.70343±1	0.70637±5	0.71056±1	0.70591±1	0.70596±1
$^{143}Nd/^{144}Nd$	–	0.512766±6	0.512778±6	0.512652±7	0.512740±5	–	–	0.512714±6	0.512993±4	0.512813±9	–	0.512373±6	0.512656±6	0.512626±6
$^{206}Pb/^{204}Pb$	–	19.145	19.153	19.112	19.148	–	–	19.153	18.946	19.084	18.869	19.370	19.176	19.189
$^{207}Pb/^{204}Pb$	–	15.658	15.671	15.655	15.681	–	–	15.667	15.627	15.647	15.672	15.734	15.675	15.692
$^{208}Pb/^{204}Pb$	–	38.895	38.936	38.854	38.957	–	–	38.929	38.647	38.810	38.671	39.258	38.962	39.023

H_2O and CO_2 by infrared spectroscopy; Li, B, and REE by ICP-OES; trace elements by ICP-MS except Zr (XRF). Abbreviations: b.d.=below detection limit (~5 ppm for XRF, ~0.1 ppm for ICP-OES); –=not analyzed. $^{87}Sr/^{86}Sr_i$ recalculated to eruption age or zircon crystallization age, respectively. Isotope errors for $^{87}Sr/^{86}Sr_i$ and $^{143}Nd/^{144}Nd_i$ are reported as 2σ measurement errors and refer to the last digit. Uncertainties on Pb isotope ratios are 0.1% (see text).

[a] Trace elements by XRF.

[b] Major elements by XRF published in Schmitt et al. (2003a).

Table 3
Melt inclusion major (EPMA) and trace element (SIMS) compositions

Sample	CM-00-02	CM-00-02	CM-00-02	CM-00-02	CM-00-02	CM-00-02
Crystal-inclusion	2-1	4-1	6-1	7-1	8-1	10-1
Bubble volume	9%	5%	6%	6%	10%	7%
wt.%						
SiO_2	75.2	74.2	74.4	74.9	74.0	74.8
TiO_2	0.11	0.10	0.11	0.07	0.15	0.08
Al_2O_3	13.3	13.9	13.8	13.5	14.0	13.4
Fe_2O_3 total	0.99	1.16	1.16	1.16	1.06	1.16
MnO	0.04	0.02	0.04	0.04	0.03	0.03
MgO	0.05	0.03	0.05	0.05	0.04	0.04
CaO	0.35	0.49	0.34	0.41	0.49	0.57
Na_2O	4.05	3.92	4.03	4.01	4.20	3.94
K_2O	5.87	6.20	6.09	5.85	5.91	5.91
P_2O_5	b.d.	b.d.	b.d.	b.d.	0.01	b.d.
H_2O	0.8	0.9	1.1	0.9	1.0	0.6
CO_2	b.d.	b.d.	b.d.	b.d.	b.d.	b.d.
F	b.d.	b.d.	b.d.	b.d.	b.d.	b.d.
Cl	0.12	0.09	0.09	0.14	0.09	0.10
Total	98.3	99.1	100.9	99.3	100.4	98.1
ppm						
Li	1095	770	1044	1213	1194	911
B	234	157	219	215	180	179
Rb	312	253	308	304	432	290
Sr	15	16	13	8	18	18
Y	21	23	22	26	19	23
Nb	10	6	7	7	6	6
Zr	128	66	78	82	79	84
Ba	211	167	107	59	265	343
La	24	23	21	27	20	24
Th	24	23	26	27	16	22
U	10	9	11	10	7	8

H_2O and CO_2 by FTIR.
Bubble volume estimated from microscopic measurement of inclusion and bubble diameters assuming spherical geometry. Abbreviations: b.d. = below detection limit (~0.01 wt.% for EPMA, ~5 ppm for FTIR).

based on their spatial proximity to the GPC. Four major observations follow from the inspection of major and trace element variations plotted against SiO_2 (Fig. 3):

(1) compositions of Cobb Mountain volcanic rocks partly overlap with the field for GPC plutonic rocks (Schriener and Suemnicht, 1980; Hulen and Nielson, 1993);
(2) whole-rock compositional trends are typically linear only within limited ranges of SiO_2 contents and an apparent flexure occurs at intermediate values (between ~60 and 65 wt.% SiO_2); this flexure is most pronounced in the Al_2O_3 vs. SiO_2 diagram (Fig. 3a), but similar observations also hold e.g., for TiO_2 and P_2O_5 (not shown), and trace elements such as Rb and Sr (Fig. 3e–f);
(3) between ~65 and ~75 wt.% SiO_2, the data show a continuous differentiation trend, and at high SiO_2 contents whole-rock analyses closely overlap with melt inclusion glass compositions;
(4) there is an apparent gap between ~50 wt.% SiO_2 (basalt of Caldwell Pines) and ~60 wt.% SiO_2 (andesite of Ford Flat). This, however, reflects the limited area of sampling and is not representative for Clear Lake volcanism in general. Note that Hearn et al. (1981) published rock analyses for the entire Clear Lake volcanic field that include numerous examples of basaltic andesite and andesite.

Trace element data normalized to primitive mantle (McDonough and Sun, 1995) are plotted in Fig. 4. For basalt of Caldwell Pines we find that, compared to primitive mantle, strongly incompatible trace elements are more enriched (~20-fold) than less incompatible trace elements such as the heavy REE (~3-fold). A characteristic negative Nb anomaly exists, whereas Pb and Sr show positive anomalies. Spidergrams for the more evolved dacitic to rhyolitic rocks also display these general characteristics and indicate even higher enrichments of incompatible trace elements that reach up to ~800-fold primitive mantle values in rhyolite of Alder Creek. Another obvious feature is that Sr, Ba, and Eu become progressively depleted in more evolved rocks (Fig. 4a). Note that strong negative Eu anomalies are uncommon in the basalts and dacites (Fig. 4b and c). By contrast rhyolite of Alder Creek displays a strong negative Eu anomaly ($Eu/Eu^* = 0.31–0.40$). Overall, REE patterns are steeper in intermediate to rhyolitic rocks (maximum $La/Yb = 14$ in rhyolite of Alder Creek) compared to basalt of Caldwell Pines ($La/Yb = 4.5$).

GPC microgranite porphyry (Fig. 4a) has characteristics similar to those of the rhyolites, such as

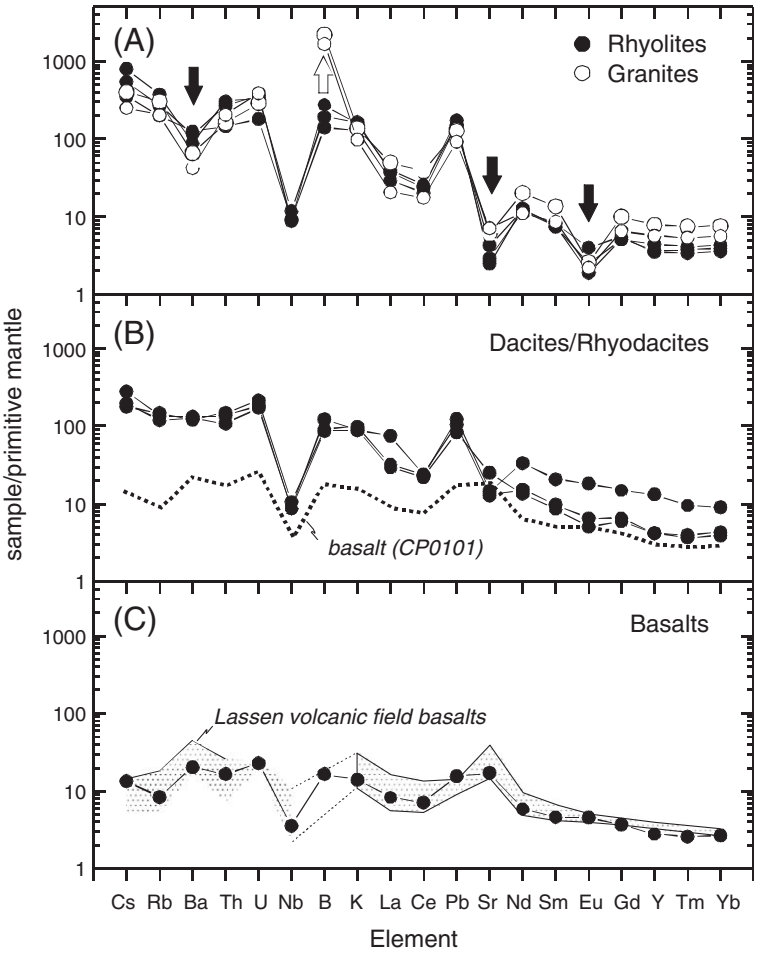

Fig. 4. Trace element abundances normalized to primitive mantle (McDonough and Sun, 1995). Note close overlap with field for selected basalts from Lassen volcanic field in 4c (data from Bacon et al., 1997; Borg et al., 1997). Solid arrows indicate depletion in feldspar-compatible trace elements for evolved compositions, and open arrow indicates selective boron enrichment by hydrothermal processes in GDC21 microgranite porphyry in 4a (see Fig. 2b).

depletion in feldspar-compatible trace elements such as Sr and Ba. This also holds for REE patterns, with the exception of sample GDC21-5865-D which displays a comparatively flat REE pattern (La/Yb=5.4). Negative Eu anomalies (Eu/Eu*=0.22–0.29) are significantly more pronounced in plutonic samples than compared to rhyolite of Alder Creek. Another difference between the plutonic samples and the rhyolites is that the former show a characteristic spike in boron (Fig. 4a). This is consistent with the petrographic observation of secondary tourmaline veinlets and suggests post-magmatic boron enrichment.

5.2. Melt inclusion major and trace element compositions

Quartz-hosted melt inclusions from rhyolite of Alder Creek in general have major element compositions that are similar to the whole-rock compositions of their host lava with the exception of alkali oxides. These are higher in melt inclusions compared to whole-rock analyses (e.g., K_2O; Fig. 3d). Major differences between melt inclusion and whole-rock compositions exist for many trace elements (Fig. 3e and f). For example, incompatible

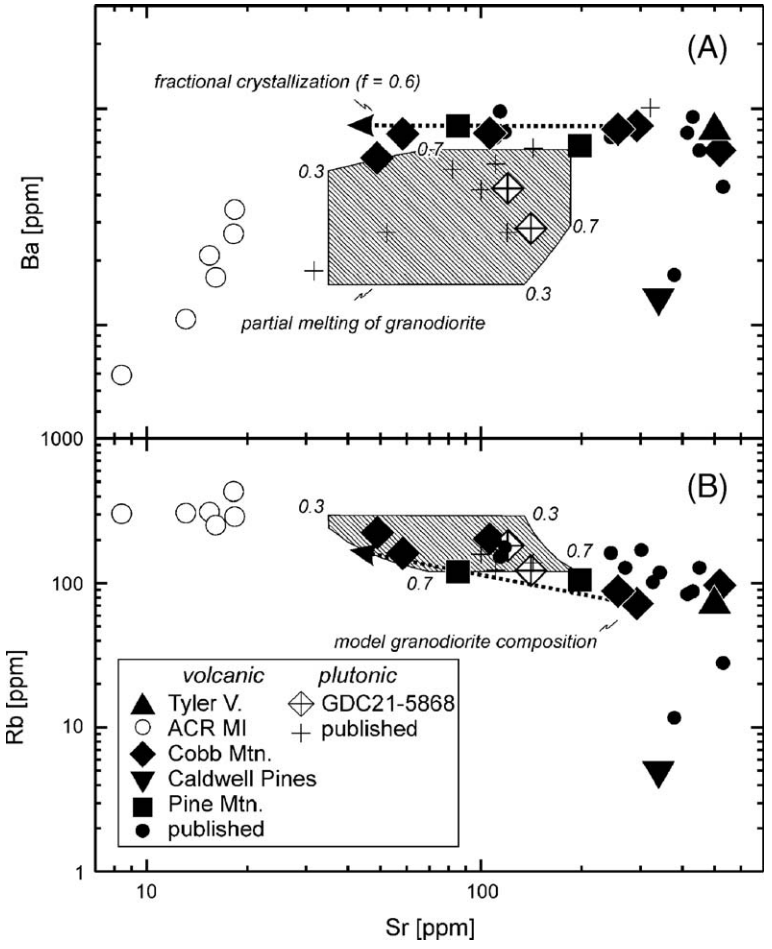

Fig. 5. Whole-rock and melt inclusion variation diagrams for selected trace elements. Abbreviations and other data sources see Fig. 3. Arrow indicates 40% fractional crystallization of rhyodacite melt (using D-values calculated from Ewart and Griffin, 1994: $D_{Sr}=5$; $D_{Ba}=0.7$; $D_{Rb}=0.1$). Hatched fields indicate partial melt compositions after 30% to 70% batch-melting of granodiorite compositionally equivalent to rhyodacite of Cobb Mountain. Range of D-values from Bacon (1992): $D_{Sr}=2.3–10$; $D_{Ba}=1.8–7$; $D_{Rb}=0.01–0.1$.

trace elements (e.g., Rb) are significantly higher in melt inclusions compared to the rhyolites (Fig. 3f). Furthermore, feldspar-compatible trace elements in melt inclusions show a change in slope on a log–log variation diagram that is steeper than the trend defined by the dacite and rhyolite whole-rocks (Fig. 5a). In this context, we reiterate that the least evolved whole-rock samples (basalt of Caldwell Pines and andesite of Ford Flat) define yet another trend, in which Ba and Sr correlate with SiO_2 (Fig. 3e).

Melt inclusions have the potential to better preserve magmatic volatile components compared to whole-rocks because their enclosure in the host mineral prevents loss of dissolved gasses. H_2O contents determined by FTIR, however, are low (~1.0–2.0 wt.%; Table 3) compared to saturation values at pressures of ~100 MPa (~4 km depth, estimated from the depth of the GPC) that are ~4 wt.% (Tamic et al., 2001). Other volatile components such as Li and B are significantly higher in melt inclusions compared to whole-rock analyses. This is particularly striking for Li which shows a 10-fold enrichment in the melt inclusions compared to values for rhyolite of Alder Creek.

5.3. Pb, Sr, and Nd isotopes

Dacitic to rhyolitic rocks have Pb, Sr, and Nd isotopic compositions that fall between those of basalt of Caldwell Pines and the regional metasedimentary rocks ($^{87}Sr/^{86}Sr$ ratios corrected to initial values; Figs. 8 and 6). Notably, all igneous samples studied are isotopically distinct from potential crustal sources although limited overlap exists in the $^{206}Pb/^{204}Pb$ and $^{87}Sr/^{86}Sr$ compositional fields for Franciscan rocks (Figs. 8 and 6; Sinha and Davis, 1971; Sherlock et al., 1995; Linn et al., 1992). Two samples of crustal rocks, one metasedimentary ''greywacke'' and one serpentinite collected few km south of Cobb Mountain are similar to the range of published values. The serpentinite sample, however, has very low abundances in Pb, Sr, and Nd, in part below detection limits. We therefore dismiss a significant role for ultramafic Franciscan rocks in the interaction of magma with preexisting crust, and will exclude them from further discussion.

On first sight there appears to be no strong correlation between isotopic ratios and degrees of fractionation (e.g., Sr abundance; Fig. 6). Closer inspection of the basaltic and intermediate rocks including the low-SiO_2 GDC21-5865 microgranite porphyry, however,

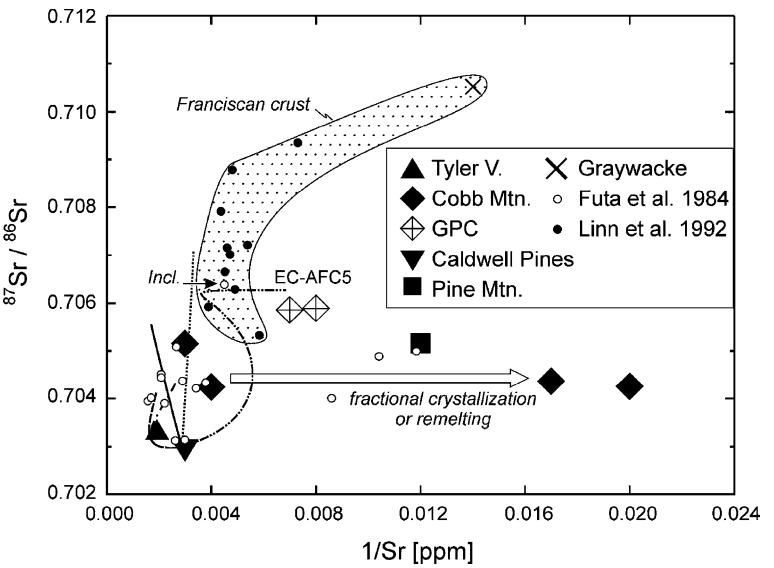

Fig. 6. $^{87}Sr/^{86}Sr$ vs. 1/Sr for Geysers volcanic and plutonic rocks. Compositions of regional crustal rocks of the Franciscan and Great Valley sequence (stippled field; data from this study, Linn et al., 1992) and values for Clear Lake volcanics (Futa et al., 1981) including a biotite schist xenolithic inclusion (Incl.) are plotted for comparison. See caption for Fig. 8 and Table 4 for EC-AFC model conditions. Large arrow represents closed-system fractionation or remelting trends to Sr-depleted compositions that cannot be reproduced by single-stage AFC models.

reveals that with increasing SiO_2, $^{87}Sr/^{86}Sr$ and $^{206}Pb/^{204}Pb$ tend to increase, whereas $^{143}Nd/^{144}Nd$ decreases. Prominent exceptions are high Si rhyolites such as Alder Creek and Pine Mountain. For example, rhyolite of Alder Creek is isotopically similar to less evolved samples such as dacite of Cobb Mountain. In a similar fashion, more evolved rocks are displaced to the right of the main field in the $^{87}Sr/^{86}Sr$ vs. $1/Sr$ diagram (Fig. 6). This observation also holds for published Sr isotopic data from a wider range of Clear Lake lavas (Fig. 6). In comparison to previously published $^{87}Sr/^{86}Sr$ ratios for GPC cuttings (~0.708; Schriener and Suemnicht, 1980), two samples of GDC21-5865 microgranite porphyry yielded distinctively less radiogenic results. Schriener and Suemnicht (1980), however, suggest that the cuttings they analyzed were contaminated by Franciscan host rocks and we therefore consider only results from uncontaminated core samples in the discussion.

6. Discussion

6.1. Rationale for petrogenetic modeling of the Geysers magma system

Isotopic variations in plutonic rocks from the Geysers and associated volcanic rocks are greater than analytical uncertainties and provide evidence that compositional variations in the Geysers magma system are not the result of closed-system fractionation within a single long-lived, continuously molten magma chamber (cf. Isherwood, 1981). Their isotopic compositions are also different from those known for regional crustal rocks (Franciscan and Great Valley sequence), which indicates that processes other than crustal melting alone must be considered. Isotopic compositions in the Geysers magma system appear to vary independently with regard to eruption or zircon crystallization ages (cf. Hammersley and DePaolo, 1999). For example, the oldest intrusive phase in the GPC, (microgranite porphyry) and the second youngest extrusive unit (dacite of Cobb Valley) have the most radiogenic Sr and least radiogenic Nd isotopic compositions, whereas rhyolite of Alder Creek and the overlying Cobb Mountain rhyodacite are intermediate in age, but have less crustally influenced isotopic signatures.

Despite the lack of a clear age progression in the composition of intrusive and extrusive magmas, the overlapping zircon age populations of GPC rocks and Cobb Mountain volcanics suggest that they are genetically closely related (Schmitt et al., 2003b). First-order observations from isotopic, major and trace element variations further guide the choice of our petrogenetic modeling:

(1) isotopic heterogeneity requires open-system processes, such as magma mixing or assimilation;
(2) breaks in slope in variation diagrams, however, rule out simple binary mixing;
(3) correlation between SiO_2 and Sr as well as lack of negative Eu anomalies imply that for basaltic to andesitic magmas plagioclase fractionation is insignificant;
(4) plagioclase fractionation appears more relevant for evolved magmas based on negative Eu anomalies in dacites and rhyolites;
(5) steeper trends in Ba vs. Sr for melt inclusions compared to dacitic and rhyolitic whole-rock trends require yet another change in the crystallizing assemblage (i.e., the presence of K-feldspar in addition to plagioclase).

Assimilation–fractional crystallization (AFC) has previously been recognized as an important process to generate compositional and isotopic variations present in Coast Range volcanic suites (e.g., Hearn et al., 1981; Johnson and O'Neil, 1984). From classical AFC parameterization, it is expected that variations of radiogenic isotope compositions when plotted against some index of differentiation (e.g., Sr abundance) follow a monotonic trend towards the composition of the contaminant (DePaolo, 1981). Fig. 6 indicates that such a trend is absent in our sample suite and literature data for Clear Lake volcanics (Futa et al., 1981). Energy-constrained AFC (EC-AFC) models (Bohrson and Spera, 2001; Spera and Bohrson, 2001), however, suggest that deviations from monotonic trends may in fact be the rule and that AFC should therefore not be ruled out for the origin of Geysers magmas. There are additional complexities in modeling AFC that can arise from the temperature and composition dependency of partition coefficients (e.g., Blundy and Wood, 1991), changes in the mode and relative abundances of crystallizing phases (see above), heteroge-

neous crustal contaminants, and post-AFC processes such as subsequent closed-system fractional crystallization or remelting. Despite these complexities, independent AFC models presented below yield consistent results for the amount of basalt required for crustal melting and hybridization (6.2), but also indicate that fractional crystallization or remelting might play a role in magmagenesis (6.3). Finally, we also use trace element and isotopic data to speculate on the potential sources of the basaltic magmas (6.4).

6.2. Basalt fractionation and assimilation of Franciscan crust

In contrast to previous AFC models (Johnson and O'Neil, 1984), we do not invoke 'hidden' crustal rocks with isotopic compositions different from those found in surface rocks. Instead we argue that surface rocks are also representative for deeper crustal levels, because the Coast Ranges crust is to a large extent formed by accretionary wedge sediments that inherited isotopic signatures of their source, the eroded portions of Cenozoic arc magmatites located to the East (Linn et al., 1992). The close Sr isotopic similarity between weakly metamorphosed Franciscan and Great Valley sequence rocks and high-grade metamorphic crustal xenolithic inclusions from Coast Range lavas implies that these xenoliths are likely Franciscan Complex rocks metamorphosed to granulite facies (Futa et al., 1981; see Fig. 6).

A second difference between our and previous AFC models for Coast Range magmas is that we use independent constrains for our "*r*-values", a critical parameter in AFC calculations describing the relative rates of assimilation and fractional crystallization (DePaolo, 1981): (1) the model by Aitcheson and Forrest (1994) that is based on solving multiple AFC equations simultaneously with r and ρ (mass ratio of assimilated material to original magma) as variables; the intersection of AFC curves in the ρ vs. r (ρ vs. or β — mass ratio of recharged material to original magma in the case of recharge) space then yielding internally consistent values for these variables; (2) the model by Spera and Bohrson (2001) that is an energy-constrained AFC (EC-AFC) parameterization in which magma crystallization, heat transfer, and crustal melting are independently calculated within a set temperature range.

We chose basalt of Caldwell Pines as our parental magma because of its close temporal and spatial relation to silicic magmatism at the Geysers. The presence of cumulate olivine and clinopyroxene phenocrysts in basalt of Caldwell Pines has only minor impact on the abundance of oxygen and trace elements relevant for our AFC models (Sr, Nd, and Pb). Magma temperatures estimated from two-feldspar and zircon saturation thermometry (800 °C; Table 1a) were used as representatives for the silicic magmas in the Geysers magma system. Calculations were performed using bulk mineral–melt D-values based on published mineral–melt partition coefficients that are consistent with first-order observations on trace element variations, and a range of crustal end-member compositions (Table 4).

Fig. 7 summarizes results for AFC model calculations using the Aitcheson and Forrest (1994) approach. Curves for four independent isotopic systems (O, Sr, Nd, and Pb) converge for ρ values (mass crust/mass original magma) between ~0.1 and ~0.4 (Fig. 7). The likely values for r are between ~0.1 and ~0.3 (no recharge) whereas the region of convergence within the β vs. r space (recharge) yields values for β in the range of 0–1.0 (not shown). The resulting rates of recharge over the rate of crystallization consequently are low and ρ values are indistinguishable to those obtained in the no recharge scenario. We will further neglect recharge because of the minor impact for the estimated ratio between basalt and assimilated crust.

Energy-constrained AFC models were set up using the same end-members as in the previous calculations and standard thermal parameters (Grunder, 1995). The estimated initial basalt temperature (1250 °C) is within the range of predicted mantle upwelling temperatures (900–1300 °C; Guzofski and Furlong, 2002). Two thermally and petrologically distinct melting scenarios were tested: EC-AFC 1 and 2 models (Table 4) assume low-pressure, low-temperature garnet-absent melting of a model biotite–gneiss, whereas EC-AFC 3, 4 and 5 are scenarios (Table 4) of high-pressure, high-temperature melting in the presence of garnet (Patiño Douce and Beard, 1995). Rare earth element ratios (La/Yb) are potential indicators for the depth of crustal melting because of the high D_{Yb} (~55) between anatectic melt and its residue in the presence of garnet.

The model corroborates the general feasibility of AFC: curves 3 and 4 bracket most isotopic composi-

Table 4
EC-AFC model parameters

Common parameters							
T_{liq}		°C					1250
T_{ini}		°C					1250
c_p		J/kg K					1100
H_{cry}		J/kg					400,000
T_{liq}		°C					700
T_{sol}		°C					1050
C_p		J/kg K					1100
H_{fus}		J/kg					300,000
Individual scenarios			1	2	3	4	5
T_{ini} crust	°C		300	300	600	600	600
Initial magma (basalt)							
	D_{Sr}		0.75	0.75	1	1	2.5
	D_{Nd}		0.3	0.3	0.4	0.4	0.3
	D_{Pb}		0.09	0.09	0.09	0.09	–
	D_{La}		0.1	0.1	0.1	0.1	–
	D_{Yb}		0.75	0.75	0.75	0.75	–
Assimilant							
	D_{Sr}		0.65	0.65	0.24	0.24	0.24
	c_{Sr}	ppm	72	205	72	205	72
	ε_{Sr}		0.7105	0.7063	0.7105	0.7063	0.7105
	D_{Nd}		1.3	1.3	0.4	0.27	0.4
	c_{Nd}	ppm	17	22	17	0.27	17
	ε_{Nd}		0.512373	0.512554	0.512373	0.512554	0.512373
	D_{Pb}		0.41	0.41	0.18	0.18	–
	c_{Pb}	ppm	9.3	9.3	9.3	9.3	–
	ε_{Pb}		19.37	19.1	19.37	19.1	–
	D_{La}		2.31	2.31	0.81	0.81	–
	c_{La}	ppm	20	20	20	20	–
	D_{Yb}		0.43	0.43	55	55	–
	c_{Yb}	ppm	1.6	1.6	1.6	1.6	–
Results							
	M_m		0.11	0.11	0.23	0.23	0.23
	M_a		0.08	0.08	0.20	0.20	0.20
	M_a/M_c		0.08	0.08	0.21	0.21	0.21
Curve in Figs. 6 and 8			dash–dot	dash	dot	solid	dash–double dot

Subscript "ini" initial (for basalt and crust), "sol"=solidus, "liq"=liquidus. H_{cry}=enthalpy of crystallization, H_{fus}=enthalpy of fusion. D=bulk mineral–melt distribution coefficient, c concentration, ε isotopic ratio. M_m=mass of remaining magma (normalized to 1 mass unit of basalt), M_a=mass of assimilated crustal melt (normalized to one mass unit of basalt), M_a/M_c=mass ratio of assimilation to crystals formed (equivalent to r). Model calculations for non-linear melt production and thermal parameters from Grunder (1995). D-values for anatectic melt calculated for melt residuals from Patiño Douce and Beard (1995) using mineral–melt partitioning coefficients from Sisson and Bacon (1992), Bea et al. (1994), and Ewart and Griffin (1994). Basalt D-values calculated using partitioning data for olivine, plagioclase and clinopyroxene complied from McKay et al. (1994), Fujimaki et al. (1984), Dunn and Sen (1994), and Hauri et al. (1994).

tions measured for Geysers igneous rocks (Fig. 8). At the equilibration temperature, the calculated mass of remaining magma relative to the original basalt is ~20% (Table 4), in close agreement with our Aitcheson and Forrest (1994) model results. An important additional observation derived from EC-AFC calculations is that initial crustal temperatures of 300 °C (~10 km depth for a geothermal gradient of 30 °C/km) are

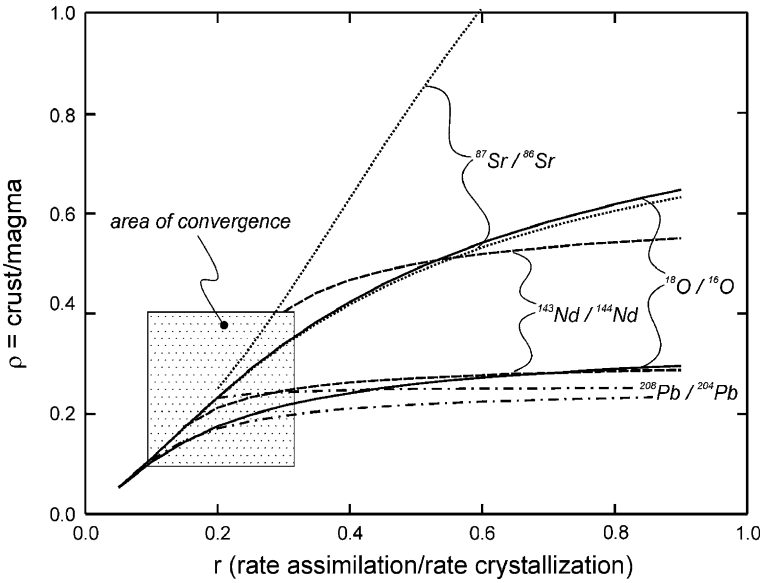

Fig. 7. Results for Aitcheson and Forrest (1994) model calculations in the ρ (crust/initial magma ratio) vs. r (rate of assimilation/rate of crystallization) space for O, Sr, Nd, and Pb isotopes. For range of D-values and assimilant compositions see Table 4; end-member compositions equivalent to CP-01-01 (basalt) and CM-00-04 (contaminated magma) from Table 2, except for oxygen isotopic compositions ($\delta^{18}O_{SMOW}$ values for assimilant = 11–15‰, basalt = 7‰, hybrid magma = 8.7‰; literature values from Johnson and O'Neil, 1984, and Lambert and Epstein, 1992).

insufficient to produce the amount of crustal melts required to match Nd and Sr isotopic compositions of the isotopically more evolved Geysers rocks, in particular the microgranite porphyry samples. Consistent with this observation is the fact that La/Yb ratios in intermediate Geysers rocks (La/Yb = 10–14) are significantly higher than predicted by garnet-absent EC-AFC trends (La/Yb < 6). This suggests that AFC presumably occurred in the presence of garnet. Patiño Douce and Beard (1995) estimated pressures >1000 MPa for garnet formation during melting of a model graywacke, somewhat higher than the range of geobarometric estimates for garnet-bearing xenoliths in Clear Lake lavas (440–760 MPa; Stimac, 1993). Despite these uncertainties, our modeling results seem to support crustal melting at the base of the crust where magmatic underplating is expected (Guzofski and Furlong, 2002). In contrast to Johnson and O'Neil (1984) who advocated a purely crustal origin for evolved (high $^{87}Sr/^{86}Sr$) Coast Range volcanic rocks, we think that this is unlikely for the GPC and related volcanic rocks given the lack of overlap with crustal isotopic compositions and the scarcity of xenocrystic zircon in these samples (<3%; Schmitt et al., 2003a).

6.3. Shallow-level magma modification: fractional crystallization in a long-lived magma chamber or remelting of intrusions

One remaining question is if a single AFC event can produce evolved magmas such as rhyolite of Alder Creek without significant change in isotopic composition compared to less evolved dacites. Such a model is tested in Figs. 8 and 6 (EC-AFC 5; Table 4). The results suggest that a combination of high D_{Sr} in the magma and low Sr in the contaminant can indeed produce a ''sigmoidal'' AFC trend that results from limited addition of crustal Sr to the magma while Sr in the magma becomes depleted due to fractional crystallization. This trend, however, is inconsistent with constraints from Nd isotopic compositions (Fig. 8). Moreover, if further assimilation of metasediments by the dacite magma had occurred, we would expect a higher proportion of crustal zircon xenocrysts in the rhyolite given the fact that the dacite magma was already zircon-saturated (Schmitt et al., 2003a), which is not observed. Alternatively, we can interpret the isotopic similarity between dacites and some rhyolites as a result of closed-system processes. Two scenarios

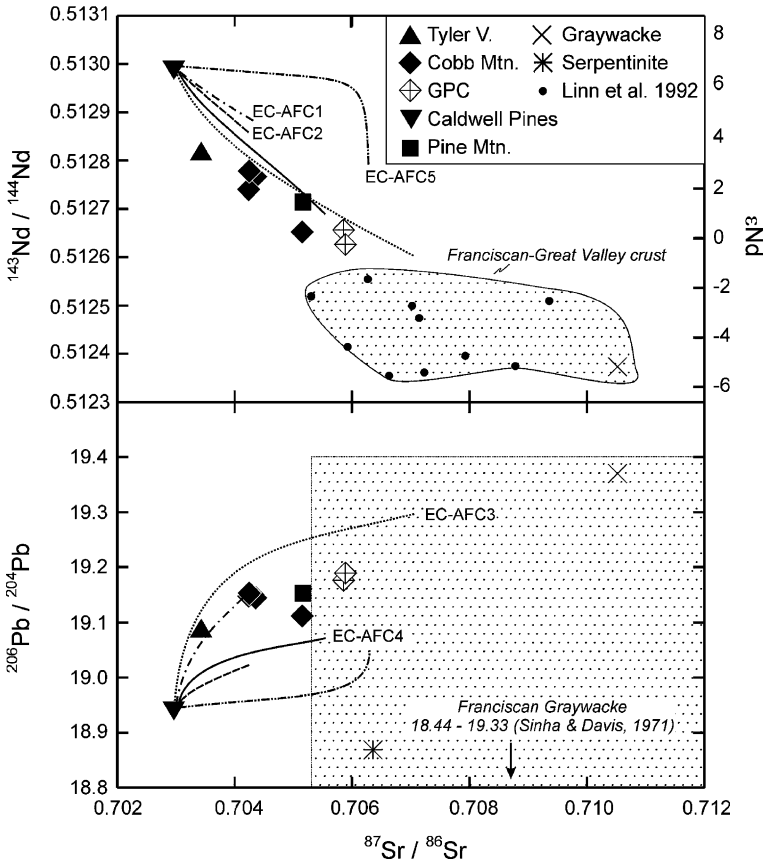

Fig. 8. $^{143}Nd/^{144}Nd$ vs. $^{87}Sr/^{86}Sr$ (a) and $^{206}Pb/^{204}Pb$ vs. $^{87}Sr/^{86}Sr$ (b) for Geysers volcanic and plutonic rocks, and regional country rocks (stippled fields). Values from this study, Sinha and Davis (1971), Linn et al. (1992); Nd and Sr data age-corrected to 1.2 Ma or eruption age. Note that Nd isotopic measurement for serpentinite was below detection limit. EC-AFC model curves 1 to 5 are plotted for two sets of assimilant compositions, initial crustal temperatures, and *D*-values for basalt and crustal partial melt (Table 4). The end of curves represents conditions at the temperature of equilibration (800 °C). Note that EC-AFC model curves 3 and 4 bracket most observed isotopic compositions of Geysers igneous rocks.

are possible: fractional crystallization subsequent to AFC or remelting of precursor intrusions. We speculate that both scenarios would likely take place at upper-crustal levels, presumably just below the intrusion depth of the GPC. Low magmatic volatile abundances in melt inclusions are in line with a shallow origin of the rhyolites, and also might be one reason for the scarcity of pyroclastic eruptions in the Geysers–Clear Lake area relative to the adjacent Sonoma volcanic field to the south (Hearn et al., 1981).

Fractional crystallization and batch-melting curves for Ba, Sr, and Rb that are based on major element least-squares (LSQ) models of a parental dacitic magma and rhyolitic daughter demonstrate the general feasibility of closed-system rhyolite generation. Using phenocryst compositions as observed in dacite lavas (see Tables 1a and b; ilmenite composition from Stimac et al., 1990, Table 2c), we calculate an amount of ~60% remaining rhyolite magma after subtraction of plagioclase (70% of the crystal phases), minor orthopyroxene (20%), ilmenite (5%), and K-feldspar (5%), with a good fit of the squared sum of residuals ($R^2<1$). Rb, Ba and Sr whole-rock compositions of rhyolite of Alder Creek also appear to be approximately consistent with ~40% fractional crystallization dominated by plagioclase (Fig. 4), but much stronger fractionation (~80%) and a change in *D*-values would be required to match melt inclusion compositions.

To test the compositional feasibility of remelting (granodioritic intrusions compositionally equivalent to

dacite of Cobb Mountain), we used effective partition coefficients from Bacon (1992) and plotted melt compositions for 30–70% partial melting in the Ba vs. Sr and Rb vs. Sr space (Fig. 5). From these results we conclude that both scenarios, fractional crystallization and remelting, are feasible in generating rhyolite from a dacitic (granodioritic) precursor. Additional considerations lead us to favor remelting of plutonic rocks as a more likely scenario: (1) melt inclusions intermediate in composition to dacite and rhyolite are lacking; this argues against a continuous fractionation history; (2) zircon ages of rhyolite of Alder Creek and the GPC closely overlap, and for a significant population predate the eruption age of rhyolite of Alder Creek by ~350 ka (Schmitt et al., 2003a). Given the relatively small volumes of erupted magma in the Geysers system, a long magma residence time is difficult to reconcile with rapid heat dissipation in shallow magma bodies (e.g., Dalrymple et al., 1999); (3) Cobb Mountain eruption ages overlap with GPC terminal K-feldspar ages (Schmitt et al., 2003b). Thus, the shallow portion of the GPC must have been already solidified when rhyolite of Alder Creek erupted, which argues against the existence of a long-lived differentiating magma chamber at shallow-levels; (4) there is petrologic evidence from other Clear Lake volcanic centers that late-stage mafic input and magma mixing occurred (Stimac and Pearce, 1992; Stimac and Wark, 1992). The presence of rare mafic crystal clots in rhyolite of Alder Creek also suggests injection and mingling with mafic magmas. We conclude that repeated thermal rejuvenation likely occurred throughout the life-span of the Geysers system.

6.4. Sources and volumes of mantle-derived magmas beneath the Geysers

There is a controversy whether basaltic melts involved in the genesis of Geysers silicic magmas were generated from depleted suboceanic asthenosphere and were modified by crustal contamination en route to surface (e.g., Cole and Basu, 1995) or if they formed in a subduction-enriched subcontinental mantle-wedge (e.g., Johnson and O'Neil, 1984; Whitlock, 2002). Validation of either hypothesis using geochemical tracers is difficult and cannot be ultimately decided here because of our very limited sampling of basaltic lavas. We note, however, that basalt of Caldwell Pines has a trace element pattern that shares many characteristic features of primitive Cascadia arc magmas (Fig. 8). This observation agrees with other examples of Coast Range basalts (Whitlock, 2002). In addition, Cascadia arc basalts and the Geysers volcanic rocks closely overlap in their Sr isotopic compositions as well as their Sr/Nd ratios (~14–70) which are higher than typical for MORB (~10). Borg et al. (1997) suggested that fluid addition caused by subduction-related devolatilization within the mantle-wedge could explain a shift from MORB compositions to high Sr/Nd values as observed in Casacade lavas. These observations lead us to propose a subcontinental mantle source for basalt of Caldwell Pines.

Based on our model results, we are now able to constrain the volume of basalt influx that is required to produce the mass of volcanic and plutonic rocks within the crustal segment beneath the Geysers. Under conditions we think appropriate for the Geysers, AFC solutions indicate that the generation of ~300 km^3 silicic magma requires ~1500 km^3 of basaltic magma (see Table 4).

Liu and Furlong (1992) and Liu (1993) estimated the thickness of a basaltic magma layer generated in a zone of mantle upwelling following the passage of the Mendocino Triple Junction to be approximately between 4 and 5 km. Little is known about the deeper roots of the GPC, but for a 10 km diameter area around the center of the GPC (~300 km^2 area equivalent to the extent of volcanic outcrop and subsurface plutonic rocks at the Geysers; see Fig. 1), this translates into a volume of underplated basalt in the order of 1200–1500 km^3 . These values are broadly consistent with our geochemical estimates for basalt fractionation, crustal melting and assimilation. Using an extrusive/intrusive ratio of 1:60 as estimated for the Geysers, ~3000 km^3 of silicic magma is predicted for in the Clear Lake area with a total erupted magma volume of ~50 km^3 (Hearn et al., 1995). This number is close to the 1000–3200 km^3 estimate based on the slabless window scenario by Liu and Furlong (1992). There would be, however, a serious discrepancy between geophysical and geochemical estimates for the amount of basalt involved in the genesis of intermediate magmas if calculations were solely based on the much smaller volumes of volcanic outcrop in the Geysers area. We therefore urge caution in the use

of "canonical" extrusive/intrusive ratios for volcanic suites where intrusive roots are unknown.

Geophysical evidence for the presence of an extensive body of mafic intrusions underlying the Geysers supports a crucial role of heat transfer by basalt ponding in the lower crust: Stanley et al. (1998) presented a three-dimensional seismic tomography model that indicates a high-velocity zone extending downward from 24 km depth under the Geysers–Clear Lake area. This zone appears separated from other bodies with high P-wave velocities that are related to ophiolitic basement rocks and was therefore interpreted as the mafic root of crustal magmatism in the Geysers region (Stanley et al., 1998). Levander et al. (1998) also described seismic reflectors below ~18 km depth in the Lake Pillsbury area south of the Mendocino triple junction, a potential analogue to the early Quaternary tectonic setting in the Geysers area.

Several recent studies aimed to reconstruct thermal histories of cooling magma bodies in the Clear Lake–Geysers area (e.g., Dalrymple et al., 1999; Norton and Hulen, 2001; Stimac et al., 2001). Regardless of the differences in how heat dissipation from intrusive bodies was modeled in detail, all authors concluded that multiple shallow-level intrusions are essential to have either sustained or reinvigorated presently observed high surface heat-flow in the Geysers–Clear Lake area. While such a scenario is consistent with the overall geochemical signature of volcanic and plutonic rocks from the Geysers, direct evidence for magmatic activity in the area of the Geysers geothermal reservoir ends with the eruption of Tyler Valley dacite ~0.7 Ma ago. Indirect evidence for recent intrusion of mantle-derived magmas is based on elevated $^{3}He/^{4}He$ and low $^{40}Ar/^{36}Ar$ ratios in the non-condensible steam phase from the northwest Geysers field (Kennedy and Truesdell, 1996). To determine when exactly the latest event of thermal rejuvenation occurred at the Geysers, low-temperature thermal history studies currently underway will play an essential role.

7. Conclusions

(1) Volcanic and subsurface plutonic rocks from the Geysers have isotopic ratios that fall between regional basaltic and crustal compositions. This indicates reactivation of essentially two major isotopic reservoirs over a ~0.8 Ma period of intrusive and extrusive activity.

(2) Two independent assimilation–fractional crystallization (AFC) models using constraints from Sr, Nd, Pb and O-isotope data yielded concordant results with regard to the mass ratios of original basalt to mass of assimilated crust (~5:1). The two end-members in this process are basalt with a geochemical signature typical for the subcontinental mantle-wedge, and crustal melts that inherited their isotopic composition from metasedimentary country rocks. To produce intermediate magmas equivalent to those erupted from Cobb Mountain, approximately 5 times the amount of basalt is required. Relatively steep REE patterns of dacitic rocks compared to local basalt (La/Yb ~10 vs. ~4.5, respectively) imply a deep-seated zone of crustal melting and hybridization where garnet is stable (>1000 MPa). This agrees with xenolith mineral compositions and textures found elsewhere in basalts and basaltic andesites within the Clear Lake area.

(3) Evolved rhyolites (whole-rocks and melt inclusions) are strongly depleted in feldspar-compatible trace elements, but whole-rocks are isotopically similar to more primitive dacites and rhyodacites. Fractional crystallization models suggest that the rhyolites represent ~30% to 40% daughter magma from a dacitic parent. Alternatively, partial melting of granodioritic precursor intrusions could have produced rhyolitic magma. The shallow intrusion depth of granodioritic and granitic magmas that form the GPC suggests that this second phase of differentiation might have occurred in the upper crust.

(4) No systematic magma evolution trend over time was detected in this subset of Clear Lake volcanic centers. This suggests that individual magma batches evolved separately despite the fact that they share a common origin in a lower crustal zone of basalt storage, differentiation and assimilation.

(5) Mass- and energy-balanced AFC model calculations suggest that the amount of silicic magmas present within the Geysers crustal segment requires lower crustal basaltic intrusions that

are broadly consistent in volume with estimates from thermal models of basalt generation in a zone of asthenospheric upwelling associated with the migration of the Mendocino triple junction (Liu and Furlong, 1992; Liu, 1993). It is a unique situation for the Geysers area that subsurface intrusive volumes are known to at least some extent. In the absence of this information and/or reliable estimates for the intrusive/extrusive ratio, strong inconsistencies would arise between geophysical and geochemical model results for the amount of basaltic magma intrusion.

Acknowledgements

We thank Rudi Naumann (XRF), Oona Appelt (electron microprobe), Peter Dulski, Knut Hahne and Heike Rothe (ICP-MS) and Jörg Erzinger of the GeoForschungsZentrum Potsdam for their generous support. We also thank Mark Walters, Tom Box and Mitch Stark at Calpine for their support during sampling and Jeff Hulen (University of Utah) for generously making drill samples available. Thanks go to the journal editor B. Edwards and the reviewers J. Donnelly-Nolan and W. Bohrson. This research was in part supported by Department of Energy grant DE-FG-03-89ER14049 and the instrumentation and facilities grant NSF grant EAR-0113563.

References

Aitcheson, S.J., Forrest, A.H., 1994. Quantification of crustal contamination in open magmatic systems. Journal of Petrology 35, 461–488.

Bacon, C.R., 1992. Partially melted granodiorite and related rocks ejected from Crater Lake caldera, Oregon. Transactions of the Royal Society of Edinburgh. Earth Sciences 83, 27–47.

Bacon, C.R., Bruggman, P.E., Christiansen, R.L., Clynne, M.A., Donnelly-Nolan, J.M., Hildreth, W., 1997. Primitive magmas at five Cascade volcanic fields; melts from hot, heterogeneous sub-arc mantle, nature and origin of primitive magmas at subduction zones. Canadian Mineralogist 35, 397–423.

Bea, F., Pereira, M.D., Stroh, A., 1994. Mineral/leucosome trace-element partitioning in a peraluminous migmatite (a laser ablation-ICP-MS study). Chemical Geology 117, 291–312.

Blundy, J.D., Wood, B.J., 1991. Crystal–chemical controls on the partitioning of Sr and Ba between plagioclase feldspar, silicate melts, and hydrothermal solutions. Geochimica et Cosmochimica Acta 55, 193–209.

Bohrson, W.A., Spera, F.J., 2001. Energy-constrained open-system magmatic processes; II, application of energy-constrained assimilation–fractional crystallization (EC-AFC) model to magmatic systems. Journal of Petrology 42, 1019–1041.

Borg, L.E., Clynne, M.A., Bullen, T.D., 1997. The variable role of slab-derived fluids in the generation of a suite of primitive calc-alkaline lavas from the southernmost Cascades, California. Canadian Mineralogist 35, 425–452.

Cole, R.B., Basu, A.R., 1995. Nd–Sr isotopic geochemistry and tectonics of ridge subduction and middle Cenozoic volcanism in western California. Geological Society of America Bulletin 107, 167–179.

Crisp, J.A., Spera, F., 1984. Rates of magma emplacement and volcanic output. Journal of Volcanology and Geothermal Research 20, 177–211.

Dalrymple, G.B., Grove, M., Lovera, O.M., Harrison, T.M., Hulen, J.B., Lanphere, M.A., 1999. Age and thermal history of the Geysers plutonic complex (felsite unit), Geysers geothermal field, California; a $^{40}Ar/^{39}Ar$ and U–Pb study. Earth and Planetary Science Letters 173, 285–298.

DePaolo, D.J., 1981. Trace element and isotopic effects of combined wallrock assimilation and fractional crystallization. Earth and Planetary Science Letters 53, 189–202.

Dickinson, W.R., 1997. Tectonic implications of Cenozoic volcanism in coastal California. Geological Society of America Bulletin 109, 936–954.

Dickinson, W.R., Snyder, W.S., 1979. Geometry of triple junctions related to San Andreas transform. Journal of Geophysical Research 84, 561–572.

Donnelly-Nolan, J.M., Hearn Jr., B.C., Curtis, G.H., Drake, R.E., 1981. Geochronology and evolution of the Clear Lake volcanics. U.S. Geological Survey Professional Paper 1141, 47–60.

Donnelly-Nolan, J.M., Burns, M.G., Goff, F.E., Peters, E.K., Thompson, J.M., 1993. The Geysers–Clear Lake area, California; thermal waters, mineralization, volcanism, and geothermal potential. Economic Geology 88, 301–316.

Dunn, T., Sen, C., 1994. Mineral/matrix partition coefficients for orthopyroxene, plagioclase, and olivine in basaltic to andesitic systems; a combined analytical and experimental study. Geochimica et Cosmochimica Acta 58, 717–733.

Emmermann, R., Lauterjung, J., 1990. Double X-ray analysis of cuttings and rock flour; a powerful tool for rapid and reliable determination of borehole lithostratigraphy. Scientific Drilling 1, 269–282.

Ewart, A., Griffin, W.L., 1994. Application of proton–microprobe data to trace-element partitioning in volcanic rocks. Chemical Geology 117, 251–284.

Fox Jr., K.F., Fleck, R.J., Curtis, G.H., Meyer, C.E., 1985. Implications of the northwestwardly younger age of the volcanic rocks of west–central California. Geological Society of America Bulletin 96, 647–654.

Fujimaki, H., Tatsumoto, M., Aoki, K.I., 1984. Partition coefficients of Hf, Zr, and REE between phenocrysts and groundmasses. JGR. Journal of Geophysical Research, B, Solid Earth and Planets 89, 662–672 (Suppl.).

Futa, K., Hedge, C.E., Hearn Jr., B.C., Donnelly, N.J.M., 1981. Strontium Isotopes in the Clear Lake Volcanics, Research in the Geysers–Clear Lake Geothermal Area, Northern California. U.S. Geological Survey, pp. 61–66.

Goes, S., Govers, R., Schwartz, S.Y., Furlong, K.P., 1997. Three-dimensional thermal modeling for the Mendocino triple junction area. Earth and Planetary Science Letters 148, 45–57.

Goff, F., Bergfeld, D., Janik, C.J., Counce, D., Stimac, J.A., 2001. Geochemical data on waters, gases, rocks, and sediments from the Geysers–Clear Lake region, California (1991–2000): Los Alamos National Lab Report LA-13882-MS.

Green, N.L., Usdansky, S.I., 1995. Ternary-feldspar mixing relations and thermobarometry. American Mineralogist 71, 1100–1108.

Grunder, A.L., 1995. Material and thermal roles of basalt in crustal magmatism; case study from eastern Nevada. Geology 23, 952–956.

Guzofski, C.A., Furlong, K.P., 2002. Migration of the Mendocino triple junction and ephemeral crustal deformation; implications for California Coast Range heat flow. Geophysical Research Letters 29, 1–4 (10.1029/2001GL013614).

Hammersley, L.C., DePaolo, D.J., 1999. Magma recharge and crustal assimilation in the evolution of the Clear Lake volcanic field, CA; an isotopic study. Abstracts with Programs—Geological Society of America 31, 353.

Hauri, E.H., Wagner, T.P., Grove, T.L., 1994. Experimental and natural partitioning of Th, U, Pb and other trace elements between garnet, clinopyroxene and basaltic melts. Chemical Geology 117, 149–166.

Hearn, B.C. Jr., Donnelly, N.J.M., Goff, F.E., 1981. The Clear Lake Volcanics; Tectonic Setting and Magma Sources, Research in the Geysers–Clear Lake Geothermal Area, Northern California. U.S. Geological Survey, pp. 25–45.

Hearn Jr., B.C., Donnelly, N.J.M., Goff, F.E., 1995. Geologic map and structure sections of the Clear Lake Volcanics, Northern California. I — 2362, U. S. Geological Survey, Reston, VA, United States.

Hulen, J.B., Nielson, D.L., 1993. Interim report on geology of the Geysers felsite, northwestern California. Transactions — Geothermal Resources Council 17, 249–258.

Hulen, J.B., Nielson, D.L., 1996. The Geysers felsite. Transactions — Geothermal Resources Council 20, 295–306.

Isherwood, W.F., 1981. Geophysical overview of the Geysers. U. S. Geological Survey Professional Paper 1141, 97–116.

Johnson, C.M., O'Neil, J.R., 1984. Triple junction magmatism; a geochemical study of Neogene volcanic rocks in western California. Earth and Planetary Science Letters 71, 241–263.

Kasemann, S., Meixner, A., Rocholl, A., Vennemann, T., Schmitt, A., Wiedenbeck, M., 2001. Boron and oxygen isotope composition of microanalytical reference materials NIST SRMs 610/612, JB-2G and JR-2G. Geostandards Newsletters 25, 405–416.

Kennedy, B.M., Truesdell, A.H., 1996. The northwest Geysers high-temperature reservoir; evidence for active magmatic degassing and implications for the origin of the Geysers geothermal field. Geothermics 25, 365–387.

Lambert, S.J., Epstein, S., 1992. Stable-isotope studies of rocks and secondary minerals in a vapor-dominated hydrothermal system at the Geysers, Sonoma County, California. Journal of Volcanology and Geothermal Research 53, 199–226.

Levander, A., Henstock, T.J., Meltzer, A.S., Beaudoin, B.C., Trehu, A.M., Klemperer, S.L., 1998. Fluids in the lower crust following Mendocino triple junction migration; active basaltic intrusion? Geology 26, 171–174.

Linn, A.M., DePaolo, D.J., Ingersoll, R.V., 1992. Nd–Sr isotopic, geochemical, and petrographic stratigraphy and paleotectonic analysis; Mesozoic Great Valley forearc sedimentary rocks of California. Geological Society of America Bulletin 104, 1264–1279.

Liu, M., 1993. Thermal–Volcanic Evolution in the Northern California Coast Ranges, Active Geothermal Systems and Gold–Mercury Deposits in the Sonoma–Clear Lake volcanic fields, California. Society of Economic Geologists Field Guide, United States, pp. 26–37.

Liu, M., Furlong, K.P., 1992. Cenozoic volcanism in the California Coast Ranges; numerical solutions. Journal of Geophysical Research, B, Solid Earth and Planets 97, 4941–4951.

McDonough, W.F., Sun, S.S., 1995. The composition of the earth. Chemical Geology 120, 223–253.

McKay, G., Le, L., Wagstaff, J., 1994. Synthetic and natural Nakhla pyroxenes; parent melt composition and REE partition coefficients. Lunar and Planetary Science Conference 25 (Part 2), 883–884.

McLaughlin, R.J., Donnelly-Nolan, J.M., 1981. Research in The Geysers–Clear Lake geothermal area, northern California. U. S. Geological Survey Professional Paper 1141, 301–316.

Moore, J.N., Gunderson, R.P., 1995. Fluid inclusion and isotopic systematics of an evolving magmatic–hydrothermal system. Geochimica et Cosmochimica Acta 59, 3887–3907.

Norton, D.L., Hulen, J.B., 2001. Preliminary numerical analysis of the magma–hydrothermal history of the Geysers geothermal system, California, USA. Geothermics 30, 211–234.

Patiño Douce, A.E., Beard, J.S., 1995. Dehydration–melting of biotite gneiss and quartz amphibolite from 3 to 15 kbar. Journal of Petrology 36, 707–738.

Sarna-Wojcicki, A.M., Meyer, C.E., Adam, D.P., Sims, J.D., 1981. Late Quaternary climate, tectonism, and sedimentation in Clear Lake, northern California Coast Ranges. Special Paper — Geological Society of America 214, 21–44.

Schmitt, A.K., de Silva, S.L., Trumbull, R.B., Emmermann, R., 2001. Magma evolution in the Purico ignimbrite complex, northern Chile; evidence for zoning of a dacitic magma by injection of rhyolitic melts following mafic recharge. Contributions to Mineralogy and Petrology 140, 680–700.

Schmitt, A.K., Grove, M., Harrison, T.M., Lovera, O., Hulen, J., Walters, M., 2003a. The Geysers – Cobb Mountain – magma system, California (Part 1): U–Pb zircon ages of volcanic rocks, conditions of zircon crystallization and magma residence times. Geochimica et Cosmochimica Acta 67, 3423–3442.

Schmitt, A.K., Grove, M., Harrison, T.M., Lovera, O., Hulen, J., Walters, M., 2003b. The Geysers–Cobb Mountain magma system, California (Part 2): timescales of pluton emplacement and implications for its thermal history. Geochimica et Cosmochimica Acta 67, 3443–3458.

Schriener Jr., A., Suemnicht, G.A., 1980. Subsurface intrusive rocks at the Geysers geothermal area, California. Abstracts with Programs — Geological Society of America. Geological Society of America (GSA), Boulder, p. 152.

Sherlock, R.L., Tosdal, R.D., Lehrman, N.J., Graney, J.R., Losh, S., Jowett, E.G., Kesler, S.E., 1995. Origin of the McLaughlin Mine sheeted vein complex; metal zoning, fluid inclusion, and isotopic evidence. Economic Geology and the Bulletin of the Society of Economic Geologists 90, 2156–2181.

Sinha, A.K., Davis, T.E., 1971. Geochemistry of Franciscan volcanic and sedimentary rocks from California. Year Book — Carnegie Institution of Washington 69, 394–400.

Sisson, T.W., Bacon, C.R., 1992. Garnet/high-silica rhyolite trace element partition coefficients measured by ion microprobe. Geochimica et Cosmochimica Acta 56, 2133–2136.

Smith, R.L., Shaw, H.R., 1975. Igneous-related geothermal systems. In: White D.E., Williams, D.L. (Eds.), Assessment of Geothermal Resources of the United States, U.S. Geological Survey Circular, vol. 726, pp. 58–83.

Smith, R.L., Shaw, H.R., 1978. Igneous-related geothermal systems. In: White, D.E., Williams, D.L. (Eds.), Assessment of Geothermal Resources of the United States, U.S. Geological Survey Circular, vol. 790, pp. 12–17.

Spera, F.J., Bohrson, W.A., 2001. Energy-constrained open-system magmatic processes; I, general model and energy-constrained assimilation and fractional crystallization (EC-AFC) formulation. Journal of Petrology 42, 999–1018.

Spera, F.J., Crisp, J.A., 1981. Eruption volume periodicity and caldera area; relationships and inferences on development of compositional zonation in silicic magma chambers. Journal of Volcanology and Geothermal Research 11, 169–187.

Stanley, W.D., Benz, H.M., Walters, M.A., Villseñor, A., Rodriguez, B.D., 1998. Tectonic controls on magmatism in the Geysers–Clear Lake region: evidence from new geophysical models. Geological Society of America Bulletin 110, 1193–1207.

Stimac, J.A., 1991. Evolution of the silicic magmatic system at Clear Lake, California from 0.65 to 0.30 Ma, Ph.D dissertation Queen's University, Kingston, Ontario, Canada, 399 pp.

Stimac, J., 1993. The origin and significance of high-grade metamorphic xenoliths, Clear Lake volcanics, California, active geothermal systems and gold–mercury deposits in the Sonoma–Clear Lake volcanic fields, California. Society of Economic Geologists Field Guide, pp. 171–189.

Stimac, J.A., Hickmott, D., 1994. Trace element partition coefficients for ilmenite, orthopyroxene, and pyrrhotite in rhyolite determined by micro-PIXE analysis. Chemical Geology 117, 313–330.

Stimac, J.A., Pearce, T.H., 1992. Textural evidence of mafic–felsic magma interaction in dacite lavas, Clear Lake, California. American Mineralogist 77, 795–809.

Stimac, J.A., Wark, D.A., 1992. Plagioclase mantles on sanidine in silicic lavas, Clear Lake, California; implications for the origin of rapakivi texture. Geological Society of America Bulletin 104, 728–744.

Stimac, J.A., Pearce, T.H., Donnelly-Nolan, J.M., Hearn, B.C., 1990. Origin and implications of undercooled andesitic inclusions in rhyolites, Clear Lake, California. Journal of Geophysical Research 95, 17729–17746.

Stimac, J.A., Wohletz, K., Goff, F., 2001. Thermal modeling of the clear lake magmatic–hydrothermal system, California. Geothermics 30, 349–390.

Tamic, N., Behrens, H., Holtz, F., 2001. The solubility of H_2O and CO_2 in rhyolitic melts in equilibrium with a mixed CO_2–H_2O fluid phase. Chemical Geology 174, 333–347.

Thompson, R.C., 1992. Structural stratigraphy and intrusive rocks at the Geysers geothermal field. Special Report — Geothermal Resources Council 17, 59–63.

Trumbull, R.B., Wittenbrink, R., Hahne, K., Emmermann, R., Buesch, W., Gerstenberger, H., Siebel, W., 1999. Evidence for late Miocene to Recent contamination of arc andesites by crustal melts in the Chilean Andes (25–26 degrees S) and its geodynamic implications. Journal of South American Earth Sciences 12, 135–155.

Walters, M.A., Combs, J., 1992. Heat flow in the Geysers–Clear Lake geothermal area of northern California, USA. In: Stone, C. (Ed.), Monograph on the Geysers Geothermal Field, Geothermal Research Council Special Report, vol. 17, pp. 43–53. Davis.

Whitlock, J.S., 2002. Evidence of a mantle wedge source for slab window volcanism in the northern California Coast Ranges. Master's Thesis, Pennsylvania State University, Park University, Park, PA, United States, 79 pp.